Chinese Journal of Chemical Engineering 85 (2025) 114–127

Contents lists available at ScienceDirect

Chinese Journal of Chemical Engineering

journal homepage: www.elsevier.com/locate/CJChE

Full Length Article

Numerical simulation analysis of particle motion behavior and key structures inside a novel cyclone separator

Jie Kou [1,2], Hang Qiu [1,2,*], Chenyang Wang [1,2]

[1] China University of Petroleum East China, Qingdao Campus, Qingdao 266580, China
[2] China University of Petroleum Huadong, Qingdao 266580, China

ARTICLE INFO

Article history:
Received 25 December 2024
Received in revised form
7 March 2025
Accepted 10 March 2025
Available online 23 April 2025

Keywords:
Particle motion
Gas–liquid–solid separation
Hydro cyclone
Integrated separation
Numerical simulation

ABSTRACT

This study proposes a novel cyclone separator with a conical inner core to enhance particle classification efficiency in oil and gas wellhead-recovered liquids. Particle motion and force dynamics are analyzed to optimize key structural parameters, including inlet diameter (D_i), overflow pipe diameter (D_e), insertion depth (L_e), and bottom flow pipe diameter (D_z). Numerical simulations employ the Reynolds stress turbulence model, SIMPLEC algorithm, and discrete phase model to evaluate separation performance in a gas–liquid two-phase system. Results indicate that a smaller D_i improves fine particle separation but increases turbulence; an optimal range of $D_i/D_c = 0.35–0.4$ is recommended. Larger D_e enhances the diversion ratio, aiding fine particle discharge ($D_e/D_c = 0.25–0.35$). Increased L_e facilitates fine particle overflow but induces vortices, whereas a smaller L_e stabilizes the bottom flow for larger particle separation ($L_e/D_c = 0.5–0.75$). A reduced D_z enhances centrifugal force and separation efficiency but may cause turbulence; an optimal D_z/D_c of 0.6–0.65 is suggested for stability. These findings provide valuable design guidelines for improving cyclone separator performance in multiphase flow applications.

1. Introduction

Gas–liquid–solid multiphase flow is now a common flow state in low-permeability oilfields, coalbed methane, and shale gas extraction. These processes present increasingly complex challenges as global energy demand rises. In oil and gas extraction processes, the gas–liquid–solid multiphase flow involved in water drives, fracturing, water injection, and oil and gas separation adds complexity to the flow and separation processes. Cyclone separators, efficient separation devices, are widely employed in the oil, gas, and chemical industries, particularly for treating oil and gas fluids containing solid particles. These separators effectively utilize centrifugal force to separate particles [1,2]. The separation efficiency of conventional cyclone separators is often limited under various operating conditions due to the nonlinearity of the flow field and the complexities of multiphase flow. This is particularly evident when separating fine particles, managing fluid disturbances, and addressing particle agglomeration, especially in separating fine particles, fluid disturbance, and particle agglomeration [3].

The primary influencing factors among the different factors (such as structural, operating, physical, and installation parameters) that affect hydro-cyclone performance are structural and operating parameters. Yang *et al.* [4] found that decreasing the size of the inlet channel leads to a reduction in maximum efficiency. This phenomenon was attributed to its effect on the natural vortex length within the gas–solid cyclone. Conversely, Elsayed and Lacor [5] noted that increasing the inlet size resulted in a lower pressure drop and overall efficiency of the gas–solid cyclone. Additionally, they discovered that changes in the inlet width had a more significant impact than adjustments to its height. Furthermore, Zhang *et al.* [6] and Yang *et al.* [7] established a strong correlation between the exhaust diameter and the vortex core within the gas–solid cyclone. The cylindrical boundary that separates the inner and outer vortices is roughly proportional to the overflow pipe diameter (D_e). Significant changes in the pressure gradient and velocity distribution result from the outer vortex's area gradually decreasing as D_e values rise. Jiang *et al.* [8] found through their research that increasing the cyclone inlet area can significantly reduce energy consumption and have little effect on separation performance. Wang *et al.* [9] studied the influence of the overflow pipe in-depth. They found that the overflow pipe's inner diameter and insertion depth significantly influenced the concentration performance, production capacity, and diversion ratio. A

* Corresponding author. China University of Petroleum East China, Qingdao Campus, China.
E-mail address: z22060033@s.upc.edu.cn (H. Qiu).

https://doi.org/10.1016/j.cjche.2025.03.015

mathematical model was created by Elsayed and Lacor [10] to optimize the geometry of a cyclone separator using the response surface methodology. The cyclone's vortex diameter, the length and diameter of the inlet section, and the overall height were used to obtain a dimensionless parameter that was the best design ratio to achieve the least pressure drop. It is shown that the performance of the cyclone is strongly dependent on the interaction between the effect of the inlet size and the diameter of the overflow pipe. Considering these findings, it is necessary to carry out further studies on the inlet diameter and the overflow pipe diameter.

The height of the cone of the cyclone separator is also an essential factor affecting the separation performance, which directly influences its performance by affecting the separation length and particle movement trajectory. The cylinder-to-cone ratio was obtained by combining the heights of the cylinder and cone. Several studies have examined the effect of the different cylinder-to-cone ratios on the overall performance of cyclone separators, including Brar *et al.* [11] under unrestricted conditions and Shastri and Brar [12] and Shastri *et al.* [13] under the restrictive condition of a fixed overall length of the cyclone separator. According to these studies, raising the barrel height significantly reduced pressure drop and marginally improved collection efficiency.

In addition to the above factors, other structural parameters such as overflow tube insertion depth (L_e), cone bottom diameter (D_z), bottom flow tube diameter (D_o), and height (L) are also related to cyclone performance. Still, they are usually considered insignificant, and several articles in the literature have investigated these parameters. Xiang and Lee [14] showed that by varying the cyclone height and the cyclone cone area, there is a significant difference in the tangential velocity at the top and bottom. The tangential velocity decreases with increasing cyclone height, so particle separation efficiency decreases. Gimbun *et al.* [15] confirmed that the collection efficiency decreases with increasing cone tip diameter due to creating a weaker vortex inside the cyclone. Hamdy *et al.* [16] investigated the effect of cyclone cone length on the gas phase flow field for six cyclone models. The cone length varied by keeping the cone diameter and angle constant in these different cyclones. They demonstrated that the pressure drop and radial and tangential velocities in the hurricane without a cylindrical section increase for a fixed cone angle.

The operating parameters affecting the separation performance include feed flow rate, feed concentration, inlet pressure, split ratio ambient pressure, *etc*. Bicalho *et al.* [17] concluded that an appropriate increase in feed flow rate can improve the separation efficiency of the cyclone, but the particle fragmentation caused by too large a flow rate increases the difficulty of separating fine particles; based on this finding, the proposed parallel cyclone can increase the flow rate while guaranteeing the separation efficiency. Kuang *et al.* [18] showed that the increase of material concentration will increase the cyclone cut particle size; the pressure drop is first reduced and then increased, which is mainly due to the decrease in internal tangential velocity caused by the reduction of centrifugal force, while the underflow discharge from umbrella to rope changes. Tavares *et al.* [19] proved that with the increase of the inlet pressure, the cut particle size and the diversion ratio decreased simultaneously. Therefore, Neesse *et al.* [20] used a high-pressure cyclone to reduce the cut size to about one micron. Yuan *et al.* [21] investigated the effect of shunt ratio on the separation efficiency and pressure drop. The results showed that the separation efficiency of the cyclone gradually increased with the increase of the shunt ratio. There was an ideal shunt ratio for the cyclone because the separation efficiency decreased rather than increased even after increasing the shunt ratio to a certain point.

In gas—liquid—solid multiphase separation, the motion law of particles can directly reflect its separation performance, so the study of the motion of particles in the cyclone field has a significant engineering value. Chandrakant R. *et al.* [22] investigated the application of a cascade cyclone separator in separating nanoscale aerosol particles through computational fluid dynamics (CFD) simulation, especially in airborne virus separation. The authors used a cascaded cyclone separator configuration (consisting of two connected cyclones) to improve nanoparticle separation efficiency significantly. The study showed that the optimized cascaded cyclone achieved a more than 93% separation efficiency at higher flow conditions. Cullivan *et al.* [23] used the CFD program FLUENT to numerically calculate the turbulent field of a cyclone utilizing a variety of turbulence models. The results demonstrated that the Reynolds stress model (RSM) performs better in turbulence simulation. On the other hand, Evans *et al.* [24] pointed out that the RSM can predict each anisotropic turbulence and all stress components effectively, and its stress transport equations accurately reflect the vortex effect. Narasimha *et al.* [25] investigated the impact of cyclone underflow orifice diameter and inlet velocity on separation efficiency and the efficiency of particle classification by using a discrete-phase model (DPM), and the predicted results in qualitative analyses agreed with the experimental results. The use of CFD in cyclone research has grown as a result of advancements in multiphase flow research and computer technology. CFD can offer more information about the flow field and particle motion inside the cyclone than experimental studies can. Another vital role of CFD is improving the performance of the cyclone separator by analyzing the effects of geometrical and operational factors. To optimize the cyclone separator's structure, including its size [26,27] and the vortex detector's entrance and exit [28,29], the researchers have run several numerical simulations.

Therefore, the core of this study is an in-depth study of particle motion behavior. The particle separation mechanism is analyzed by simulating the particle trajectories, velocities, and forces inside the cyclone separator, combined with the distribution characteristics of the flow field. This knowledge of particle motion behavior led to an investigation into how the cyclone separator's major structural parameters—such as the inlet diameter, overflow tube diameter, cone section length, and cone section diameter—affect particle separation efficiency. The study shows the velocity distributions, pressure contours, and particle trajectories within the device, leading to a better understanding of the separation process within the device.

2. Structure of the Cyclone Separator

In the field of gas—liquid—solid multiphase separation, degassing and desanding typically require the traditional cyclone separator to be used in steps through multiple devices, increasing process complexity and energy loss. To solve this problem, scholars have designed a multiphase separator device that integrates degassing and desanding functions, as shown in Fig. 1(a). The device achieves efficient preliminary gas—liquid separation by optimizing the flow field design so that the mixed fluid enters the cyclone and separates the gas phase first, followed by the downward movement of the liquid—solid mixture.

In the improved inner cone cyclone separator design proposed in this paper, the double cone structure and tangential inlet optimization technique are further adopted, as shown in Fig. 1(b). The double cone structure increases the effective rotating area of the cyclone, resulting in enhanced centrifugal force of the fluid within the cone section, which improves the separation efficiency of large particles. The more potent centrifugal force helps to accelerate the migration of particles towards the outer wall,

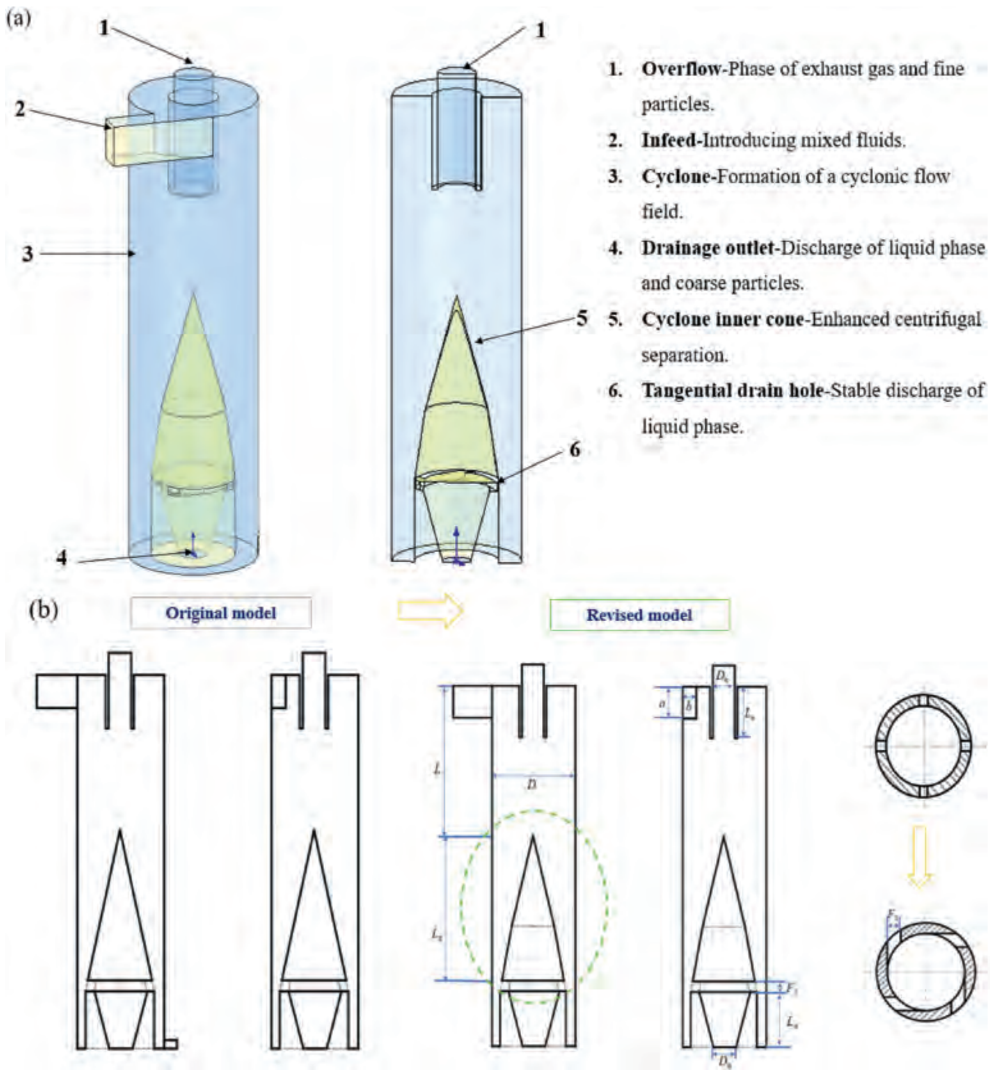

Fig. 1. Structural diagrams of (a) desanding and (b) separating device.

especially when the particles are large, and is effective in separating them from the gas–liquid–solid mixture; the double cone structure improves the stability of the fluid within the cyclone, especially in the outlet region of the separator. By adjusting the fluid path, the double-cone design reduces the occurrence of local turbulence. It provides significant benefits in multiphase flow treatment and fine particle separation by maintaining fluid homogeneity, which enhances the radial migration efficiency of the particles and lowers the likelihood of remixing the particles. The tangential discharge orifice design maintains the rotational flow state of the liquid into the bottom flow chamber and reduces the disturbance of the main cyclonic field when the fluid enters the bottom flow chamber directly. By reducing the likelihood that the liquid phase will disrupt the main flow field, this design makes sure the separator maintains a stable cyclonic structure in the downstream region of the liquid–solid separation, improving the separation efficiency.

3. Numerical Methods Description

The cyclone separation unit's particle separation and kinematic characteristics were investigated using the Eulerian multiphase flow and particle flow model (CFD–DPM). The Reynolds stress model (RSM) was selected for the turbulence model.

3.1. Turbulence model

The RSM, the RNG $k-\epsilon$ model, and the standard $k-\epsilon$ model are Fluent's three most widely used turbulence models. The standard $k-\epsilon$ model is the simplest turbulence model, and its convergence and computational accuracy can meet the requirements for general engineering calculations. Still, it does not work well in simulating complex flows such as cyclonic and bypassing flows. The RNG $k-\epsilon$ model can simulate complex flows such as jet impingement, separating, and cyclonic flows. Still, it cannot accurately predict the motion of an intense cyclone due to the limitation of the assumption of the viscous homogeneity of the swirling vortex. The most sophisticated model in Fluent is the RSM model, which accounts for the anisotropy of the RSM and the effects of rotation, bending, and vortices on the flow. It can also better predict complex three-dimensional flows, including strong cyclonic flows [30].

A specific expression of the RSM is given in the form of Eq. (1):

$$\frac{\partial}{\partial t}\rho\overline{u_i'u_j'}+\frac{\partial}{\partial x_k}\left(\rho U_k\overline{u_i'u_j'}\right)=D_{ij}^{\mathrm{T}}+D_{ij}^{\mathrm{L}}+P_{ij}+G_{ij}+\phi_{ij}+\varepsilon_{ij}+F_{ij} \tag{1}$$

where C_{ij} is the convection term; ${D^{\mathrm{T}}}_{ij}$ is the turbulent diffusion term; ${D^{\mathrm{L}}}_{ij}$ is the molecular diffusion term; P_{ij} is the stress generating term; G_{ij} is the buoyancy generating term; ϕ_{ij} is the pressure strain term; ε_{ij} is the diffusion term; and F_{ij} is the rotational generating term of the system. Where D^{T}_{ij}, G_{ij}, ϕ_{ij}, ε_{ij} need to be modeled to close the equations.

Where the molecular viscous diffusion term is shown in Eq. (2):

$$D_{ij}^{\mathrm{T}}=\frac{\partial}{\partial x_k}\left(\frac{\mu_{\mathrm{t}}}{\sigma_k}\frac{\partial\overline{u_i'u_j'}}{\partial x_k}\right) \tag{2}$$

The pressure strain term is shown in Eq. (3):

$$\phi_{ij}=\phi_{ij,1}+\phi_{ij,2}+\phi_{ij}^{w} \tag{3}$$

The buoyancy-induced generation term G_{ij} is given in Eq. (4):

$$G_{ij}=\beta\frac{\mu_{\mathrm{t}}}{P_{ij}}\left(g_i\frac{\partial T}{\partial x_j}+g_j\frac{\partial T}{\partial x_i}\right) \tag{4}$$

If the shear generation term P_{ij} is neglected, this results in a closed set of Reynolds stress equations.

The RSM model constitutes a closed N—S equation in the three-dimensional flow, which can more accurately simulate the strong cyclonic flow in the internal flow field of the cyclone separator, so the RSM turbulence model is chosen for the numerical simulation of the turbulence model in this paper.

3.2. Continuous phase model

The Euler—Lagrange and Euler—Euler methods are the two computational treatments for multiphase flows currently offered by CFD. Three Fluent multiphase flow models, the volume of fluid (VOF) model, the mixture model, and the Euler—Euler method based on this technique. The VOF model is typically used for laminar flow, wiggling, and perfusion, and it can be used to determine the interfaces between multiple immiscible media. For gas—liquid flows, the mixture model is more straightforward and effective than the conventional VOF model, which works best for two-phase flows with clearly defined interfaces. In contrast, the mixture model is ideal for a broader range of multiphase flow scenarios, especially in complex rotating flow fields such as cyclone separators, and can better simulate the mass, momentum, and energy exchange of fluids. The Eulerian model is the most complex of the three multiphase flow models, requiring the development of multiple momentum equations and continuity equations to solve for each phase. The momentum exchange between phases is related to the type of mixture, which is generally used in fluidized beds, bubble columns, particle suspensions, *etc.* [31].

This paper uses the mixture model—which has a small calculation volume and strong computational stability—to describe the gas—liquid non-uniform flow in the conical three-phase separator. It can capture the coupling between phases and is appropriate for phase mixing or phase separation in the flow.

3.3. Particle phase model

A suitable simulation method is required to study gas—solid two-phase simulation and calculate the cyclone separator. The DPM is highly suitable for simulating solid particles for sand particles with smaller particle sizes and lower concentrations. Because the concentration of the particle phase studied in this paper is less than 10%, the collision between the particles can be ignored in the control equation and momentum equation. There are two methods to solve the trajectory of solid particles in the DPM model: the cloud orbit method and the random orbit method; the principle of the cloud orbit is to track and count the particles in the turbulent diffusion by using the statistical method; the random orbit is to consider the interrelationships between different eddies through the study of vortices, which can be realistically calculated by using the random orbit. In contrast, random orbits are primarily used to investigate eddy currents and take into account the interactions between various eddy currents. These orbits can accurately depict the shifting paths of the particles' turbulent motion [32].

(1) Particle trajectory

The equations of motion of the particles in the Lagrangian coordinate system are derived from the conditions of force equilibrium for solid phase particles:

$$\frac{\mathrm{d}u_{\mathrm{p}}}{\mathrm{d}t}=F_{\mathrm{D}}\left(u-u_{\mathrm{p}}\right)+g_x\left(\rho_{\mathrm{p}}-\rho\right)/\rho_{\mathrm{p}}+F_x \tag{5}$$

$$\begin{cases} F_{\mathrm{D}}=\dfrac{18\mu}{\rho_{\mathrm{p}}D_{\mathrm{p}}^2}\dfrac{C_{\mathrm{D}}Re}{24} \\ Re=\dfrac{\rho D_{\mathrm{p}}\left|u_{\mathrm{p}}-u\right|}{\mu} \\ C_{\mathrm{D}}=\alpha_1+\dfrac{\alpha_2}{Re}+\dfrac{\alpha_3}{Re^2} \end{cases} \tag{6}$$

where u_{p} is the flow velocity of solid particles, $\mathrm{m\cdot s^{-1}}$; u is the velocity of continuous phase fluid, $\mathrm{m\cdot s^{-1}}$; ρ, ρ_{p} is the density of constant phase, solid particles, $\mathrm{kg\cdot m^{-3}}$; D_{p} is the diameter of particles, m; g_x is the acceleration of gravity in the x direction, $\mathrm{m\cdot s^{-2}}$; μ is the coefficient of viscosity, $\mathrm{Pa\cdot s}$; F_x is the external force acting in the x direction such as the mass force, thermophoretic force, *etc.*, N; Re is the Reynolds number; C_{D} is the drag coefficient; α_1, α_2, α_3 are constants, given according to the results obtained from the experiments with smooth spherical particles.

The discrete phase particle motion orbits can be derived by solving the above differential equations for the calculations.

(2) Multiphase coupling

The interaction between the gas—liquid—solid phases must be considered when calculating the particle trajectories in the cyclone separator's internal flow field using the CFD—DPM numerical simulation method. This paper only examines the coupling effect for gas—liquid two-phase systems; the interaction between the particles due to flow field changes is minimal; trajectory tracer particles can be reached in the flow field to join the source of particles by reaching stable, solid particles in the inlet. In Fluent software, the three-phase coupling steps are as follows.

① Upon stabilization of the iterative convergence results for the continuous phase flow field (excluding the solid particle phase);
② To determine the orbital solution for the solid particles entering the cyclone separator's interior at the inlet, introduce the CFD—DPM model;
③ Correct the current continuous phase and compute a new continuous phase corrected flow field by performing secondary calculations on the continuous phase flow field using the outcomes of the solved heat, momentum, and mass exchange term data;
④ Continuing the iterative calculation, the particle trajectory equations of the corrected continuous phase flow field are corrected again to obtain the latest particle motion trajectories;
⑤ Repeat steps ③ and ④ until the solution converges.

3.4. Calculation method and boundary conditions

The following settings are examined in this paper because the choice of control parameters has a significant impact on the numerical results: the solver is selected based on the pressure-based solution method, and the pressure–velocity coupling adopts the SIMPLEC algorithm with faster convergence according to the characteristics of strong cyclonic flow in the flow field inside the cyclone separator, it is more appropriate to select PRESTO! as the pressure interpolation format; the commonly used discrete formats generally include the first-order windward format, second-order windward format, QUICK differential format, and center differential format [33]. The most popular discrete formats are QUICK center differential, first-order windward, and second-order windward [33]. This paper uses the QUICK differential format because it is the most appropriate among them for simulating strong rotating flow.

Assuming that the gas–liquid–solid three-phase mixing is uniform, the inlet boundary adopts the velocity inlet, and the size is initially set to 3 $m\cdot s^{-1}$. The water and gas phases are continuous; the first phase is the water phase, the second is the gas phase at the inlet, and the particles are the discrete phase. As per the practical implementation of gas drive extracted liquid treatment, the mixed liquid's solid content is 1%, and its gas content is 59.4%. The simulation parameters were set as follows: liquid density $\rho_l = 999.85\ kg\cdot m^{-3}$, liquid dynamic viscosity $\mu_l = 3.42$ mPa·s; gas density $\rho_g = 0.6239\ kg\cdot m^{-3}$, gas dynamic viscosity $\mu_g = 1.78 \times 10^{-2}$ mPa·s; solid density; $\rho_s = 2.33 \times 10^3\ kg\cdot m^{-3}$, solid dynamic viscosity $\mu_s = 1.72 \times 10^{-2}$ mPa·s. The gravitational acceleration $g = 9.8\ m\cdot s^{-2}$ was set in the negative direction of the z-axis. The boundary conditions were set as follows.

(1) Inlet conditions: the three-phase mixture is uniform; the inlet gas mixture is assumed to flow perpendicular to the inlet cross-section.
(2) Outlet conditions: The outlet flow is assumed to be fully developed. The reference pressure (overflow port and underflow port) is set to atmospheric pressure, and the boundary condition of escape (escape) is set for solid matter in the particle phase.
(3) Wall boundary conditions: no slip and the bottom boundary of the discharge port is set to trap (trap) the solid matter of the particle phase and stop tracking when the particle phase arrives. And the wall surface boundary is set as the complete reflection (reflect) of the solid matter in the particle phase.

3.5. Grid delineation and independence verification

The Fluent pre-processing program ICEM is used to perform the mixed meshing of the separator's inner flow channel. Considering the complexity of the inner cone structure and the structure at the guide hole, a tetrahedral unstructured mesh is used to mesh the inner cone and the guide structure and encrypted appropriately to improve the computational accuracy, and a hexahedral structured mesh is used to mesh the rest of the parts. The separator mesh model is shown in Fig. 2 (see Fig. 3).

A polyhedral mesh must be created and used in the simulation for an accurate solution (see Table 1). This mesh type is generated directly by forming polygons around each node of the tetrahedral mesh, creating an appropriate mesh to solve the governing equations. This mesh type uses specific criteria to optimize judgment during generation. It can generate a high-quality mesh and make it easy to control the mesh size and node density. It has the advantages of fast convergence, high convergence accuracy, and low residual values [34]. The pressure drop and separation efficiency are

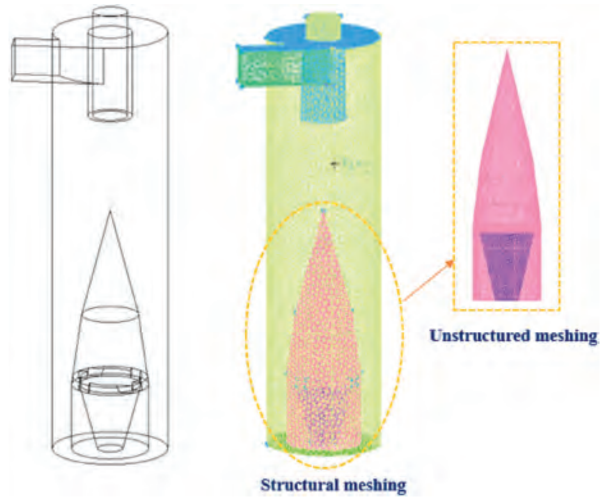

Fig. 2. Inner cone cyclone mesh division model.

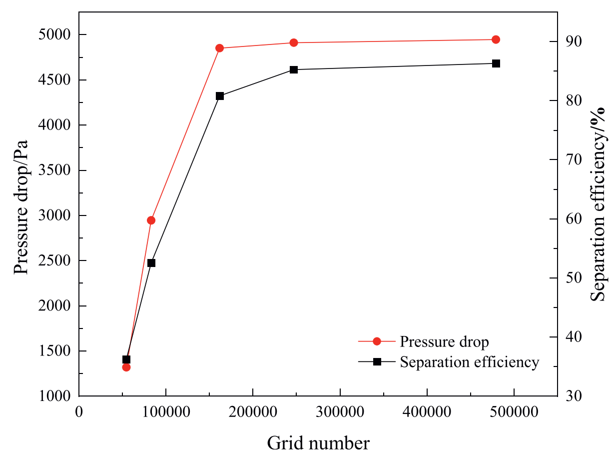

Fig. 3. Verification results of grid independence.

selected as the evaluation indexes for mesh independence verification. The validation results are shown in Table 2.

The accuracy of the simulation results and calculation time are affected by the number of grids in the numerical simulation's calculation area. It is necessary to verify the model's grid independence to determine the most appropriate number of grid divisions, reduce the calculation time, and improve the accuracy of the calculation results. The grid division for the internal cone structure of a cyclone separator was completed in this section. The analysis demonstrates that the model's five grid number levels produced a consistent pressure drop and separation efficiency distribution. When the number of grids is increased from the first to the third level, the variables change significantly.

In contrast, the simulation results of the number of grids at the third, fourth, and fifth levels are almost unchanged. For the fourth and fifth levels of grids, the device's performance is not significantly affected by the number of grids, but the calculation time increases significantly. The third-level grid is selected to improve the efficiency of the subsequent simulation computation.

4. Results and Discussion

4.1. Flow field properties

The flow field characteristics were systematically examined to understand the device's separation mechanism better. A $Z = 0$ mm

Table 1
Structural dimensions of the desanding and separating device.

Structural parameter	Value	Function
Main body diameter, D_c/mm	75	Determines the spatial distribution of particle flow and overall airflow
Inlet length, a/mm	24	Influence the velocity and flow field distribution of the feed fluid
Inlet width, b/mm	16	Influence the fluid's flow properties as it passes through the separator
Overflow diameter, D_e/mm	22.5	Determines the emission rate of gases and fine particles
Underflow diameter, D_o/mm	16.5	Primary control of larger particle size emissions
Overflow tube depth, L_e/mm	56.25	Influence on gas separation effect and adjustment of split ratio
Cylindrical section length, L/mm	131.25	Directly affects fluid rotation time and particle centrifugal force
Conical section length, L_z/mm	112.5	Regulates the degree of compression of the fluid in the separator and the efficiency of particle separation
Conical section diameter, D_z/mm	48.75	Influence on fluid flow rate and radial migration of particles
Liquid-collecting chamber height, L_o/mm	43	Determines the residence time of the fluid at the bottom flow outlet
Slot width, F_1/mm	5	Influence on fluid flow state and particle separation
Slot height, F_2/mm	5	Influence the efficiency of fluid–particle separation
Number of slots, F_3/mm	4	Determine split ratio and particle emission uniformity

Table 2
Verification results for grid independence.

Grid level	Grid number	Pressure drop/Pa	Separation efficiency/%
Level 1	54630	1320.12	36.24
Level 2	83094	2945.36	52.56
Level 3	161790	4850.71	80.83
Level 4	246989	4911.32	85.26
Level 5	479381	4945.68	86.33

cross-section and five representative cross-sections in the y-direction (Fig. 4) were chosen for flow-field analysis. In accordance with the distribution trend of tangential velocity, the pressure distribution (Fig. 5(a)) shows a monotonically decreasing characteristic from the cylinder wall to the axial direction. The centrifugal force causes the gas and liquid phases to separate, resulting in a distribution of pressure that is low in the center and high at the edges in various cross-sections. The gas phase gathers in the central low-pressure area, while the centrifugal force forces the denser liquid phase towards the vessel wall. The central low-pressure region, which is crucial for of forming gas nuclei during the gas–liquid separation process, is greatly expanded, particularly at the cyclone's bottom (conical area).

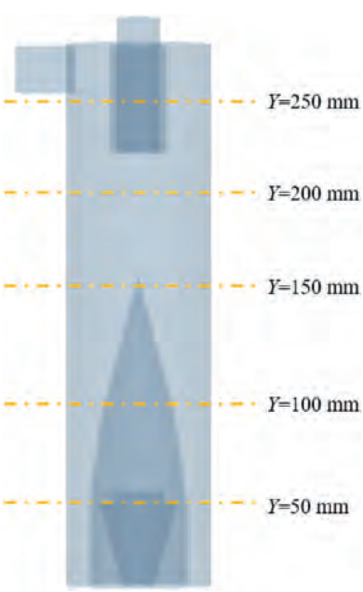

Fig. 4. Flow field monitoring surface of the cyclone separation device.

From the central axis to the vessel wall, the tangential velocity (Fig. 5(b)) progressively rises with radial distance before peaking close to the wall. The cyclonic field is gradually strengthened in the inner cone portion, which creates a strong centrifugal force that causes the solid-phase particles to migrate toward the wall, creating a demarcation between the quasi-free vortex and forced vortex regions. The gradual increase in the region near the cone in the axial direction indicates this.

The axial velocity distribution (Fig. 5(c)) depicts the typical bidirectional flow characteristics inside the cyclone. The negative axial velocity near the wall drives the liquid phase to exit towards the bottom outlet for gas–liquid separation, while the positive axial velocity flow in the center region carries the gas phase away. The distribution of positive and negative axial velocities exhibits a progressive asymmetry along the axial direction from top to bottom, suggesting a more distinct separation of the gas and liquid phases.

The following crucial mechanism governs the separation performance in addition to the cyclone separator's internal flow field characteristics: A low-pressure gas nucleus forms at the center, while the liquid-phase particles are driven towards the wall by a highly effective pressure gradient. The liquid phase can be separated effectively with a strong tangential velocity field and increased centrifugal force, but turbulence-induced flow field instability must be prevented. The gas and liquid phases are released through distinct outlets due to the steady distribution of axial velocities in both flow directions, guaranteeing separation stability and efficiency.

4.2. Kinematics of particle separation

4.2.1. Particle swarm motion analysis

The predicted trajectory distributions of various-sized particles inside the cyclone separator are shown in Figs. 6 and 7, conversely, depicts the dynamic time-varying distribution properties of the particle phase within the cyclone. The figure illustrates how the combined forces of centrifugal and trailing forces impact the particles differently after they enter the cyclone, leading to notable variations in their separation behavior and trajectories. In the pre-aligned region of the column section, the coarse particles with sizes of 30–60 μm rapidly migrate radially to the cyclone wall due to the dominant role of centrifugal force, follow a stable spiral path downward, and are finally discharged through the underflow outlet. In contrast, fine particles of 0–10 μm size are mainly affected by fluid viscous force and adsorption in the low-pressure region of the vortex nucleus, and their movement paths are concentrated around the vortex nucleus region and spiral up along the central

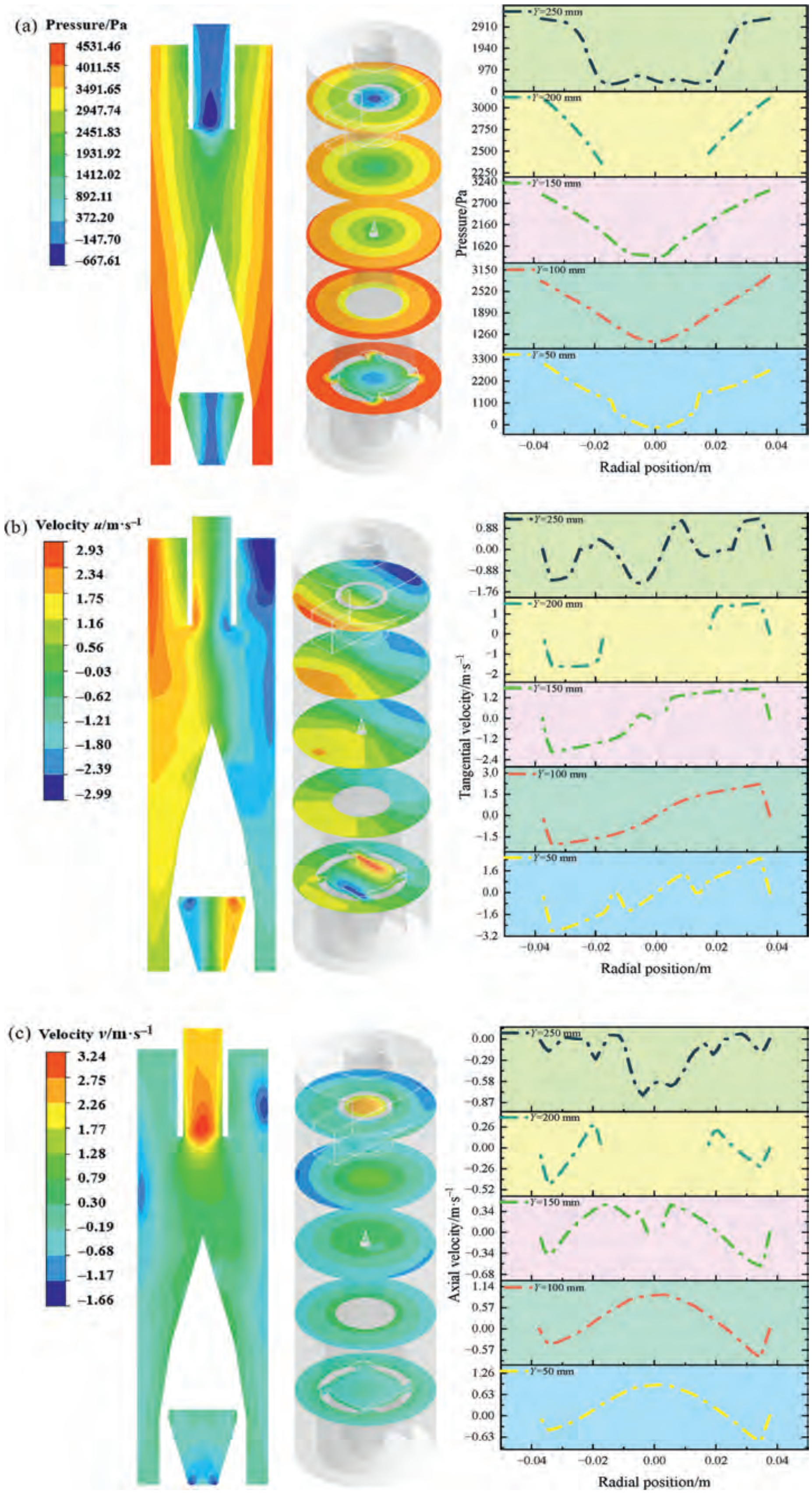

Fig. 5. Pressure (a) and tangential (b) and axial (c) velocity distributions of inner cone cyclone.

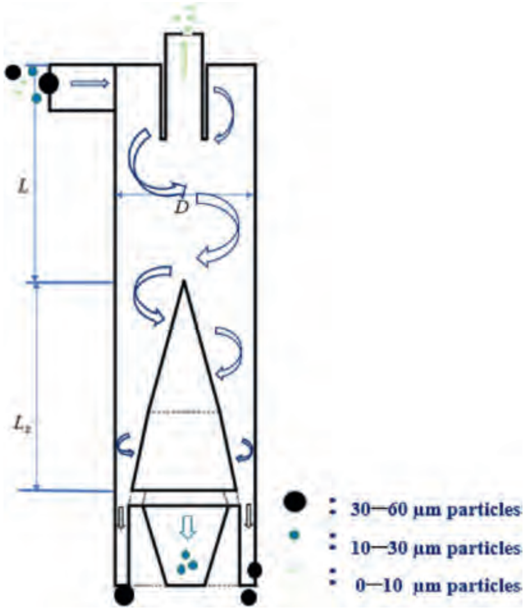

Fig. 6. Predicted particle trajectories for the cyclone separator.

axis and finally discharged through the overflow outlet. The distribution of medium-sized particles in the range of 10–30 μm is complex due to the equilibrium of the radial synergetic forces. Some particles migrate radially to the wall and move toward the bottom outlet. In contrast, others are disturbed in the vortex core region and undergo a short retention period before being guided to the bottom or overflow outlets, respectively.

4.2.2. Separation efficiency analysis

Fig. 8 shows the separation efficiency curves of different particle sizes in experimental and simulated cases, from which it can be seen that there are apparent differences in the separation efficiencies of varying particle sizes. The improved model significantly improves the separation performance compared to the original model in the range of fine particles (0–10 μm) and medium particles (10–30 μm), especially for fine particles, and is in high agreement with the experimental particle size separation efficiency curves derived by Tang [35]. This result suggests that optimizing

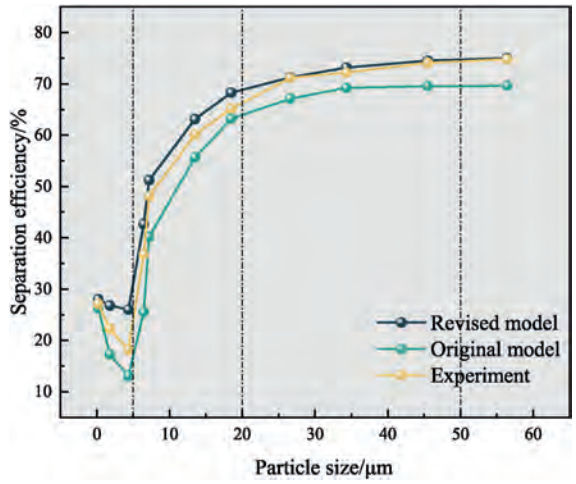

Fig. 8. Separation efficiency curves for different particle sizes.

the cone geometry and the flow field distribution of the improved model effectively enhances the adsorption of fine particles in the vortex core region and reduces the interference of fluid turbulence on the particle separation path. For large particles (>30 μm), the separation efficiencies of both models are close to 100%, indicating that the separation process is dominated by inertial force and centrifugal force, and the effect is stable. The enhanced models' notable advantages confirm the effectiveness of their ideal design in separating particles of varying sizes.

4.2.3. Particle mechanical behavior analysis

Three ranges of particle sizes were examined from the position of motion (Fig. 9(a)), the velocity of motion (Fig. 9(b)), and the force applied (Fig. 9(c)) in order to examine the motion behavior of various particle sizes inside the separator. Particles measuring 0–10 μm and 10–30 μm enter from the center of the separator's inlet, as shown in figure. A short-circuit flow forms straight from the overflow pipe because of the small particles' easy movement towards the axis due to the relatively large centrifugal buoyancy force they receive. Particles did not migrate to the separator's wall, as evidenced by the maximum radial movement of 25.3 mm into the separator. Turbulence increases before the fine particles reach the overflow pipe's outer wall surface, causing significant force and

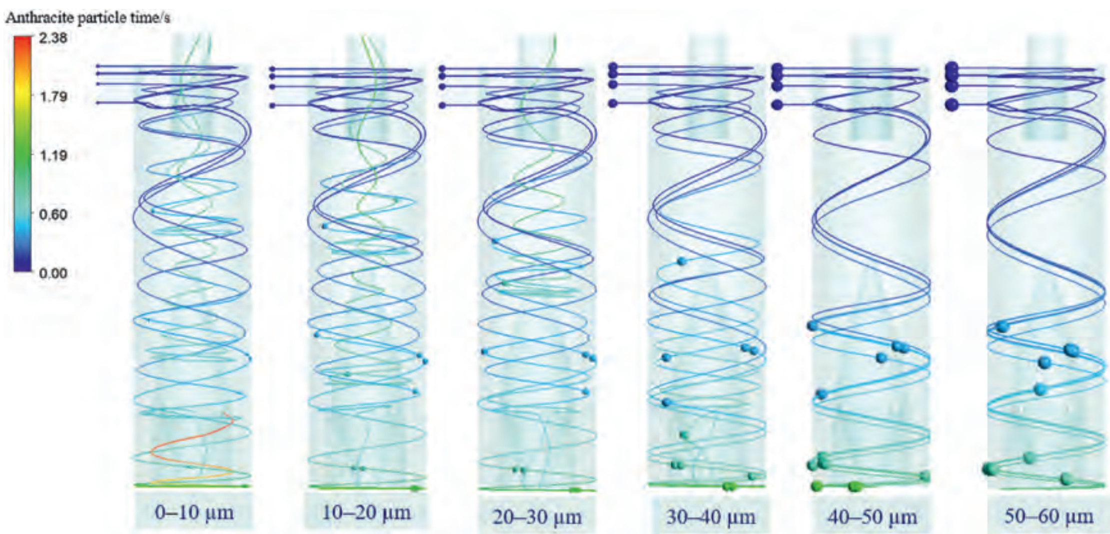

Fig. 7. Residence time-colored particle trajectories.

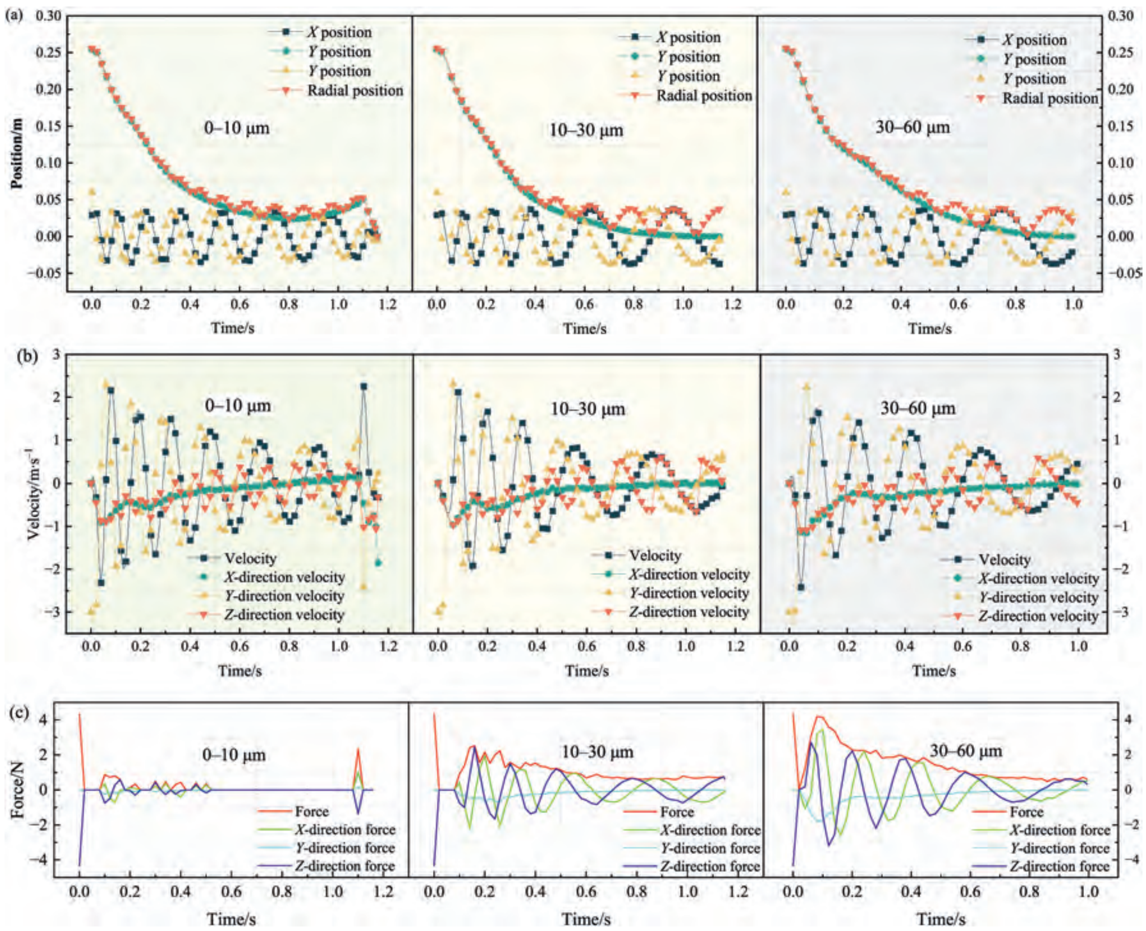

Fig. 9. Changes in (a) particle position, (b) velocity, and (c) force for three grain sizes.

velocity fluctuations in all directions. Since the cut-size particles do not collide with the wall surface, there is no point at which the particle force suddenly increases. When examining the shift in coarse particles, it is evident that the total force is greater and that the particles are moving in the direction of the wall. Most coarse particles leave the flow by radial movement to the bottom of the mouth because the centrifugal force has a stronger role in the radial direction than both the fluid trailing force and the pressure gradient force. The fluid trailing force remains the main force of particle movement in the tangential and axial directions.

Three different particle sizes' mechanical motion behavior is examined; the force and motion behavior of fine and coarse particles are more intuitive and predictable, whereas the motion of cut-size particles (10–30 μm) is more influenced by the fluid's motion state, turbulence, and eddy currents created by the abrupt change in geometry. For this reason, the impact of important structural parameters on the cut-size particle separation efficiency is further examined.

4.3. Effect analysis of structural parameters

4.3.1. Effects of D_i

The impact of dimensionless inlet diameter (D_i/D_c) on the cyclone's internal velocity field is shown in Fig. 10. Because of the decreased rotational intensity with the smaller inlet diameter, the overall separation effect is weaker, as illustrated by the curves' lower tangential velocities at lower D_i/D_c in Fig. 10(a). The rotational flow is more intense, and the overall velocity profile is higher at larger D_i/D_c. According to analysis, this is because a larger inlet diameter lowers the resistance in the in-flow region, increasing the fluid's flow velocity in the outer region. Particle–fluid interaction intensifies turbulence, particularly in the area near the device's outer diameter, where the particles are subjected to higher centrifugal force, resulting in intricate interphase coupling effects.

The features of the axial velocity distribution in a gas–liquid–solid or cyclone multiphase separation plant are depicted in Fig. 10(b). Varying D_i/D_c ratios greatly impact the fluid's velocity field. The high-velocity axial flow in the center region partly causes the expulsion of the light phase. By contrast, the outer-wall region's low-velocity reflux helps the heavy-phase particles settle and separate.

The impact of dimensionless inlet diameter (D_i/D_c) on the pressure and partition ratio is shown in Fig. 11(a). The partition ratio falls with increasing D_i/D_c, suggesting that more heavy phases are released from the bottom flow opening as pressure rises sharply. Increased internal pressure strengthens the centrifugal force field that aids in separating phases with larger density differences by increasing the cyclone separator's rotational intensity. Compromise, however, excessive pressure can also result in intense turbulence, which can compromise the equipment's stability and effectiveness. According to Fig. 11(b), the separation efficiency of small particles (less than 20 μm) is higher at smaller D_i/D_c ratios (*e.g.*, 0.2 and 0.35), and the separation is more stable in the particle size section below 20 μm. At larger D_i/D_c ratios (*e.g.*, 0.45 and 0.5), the separation efficiency of small particles is lower, and it only gradually improves with the increase of the particle size and approaches saturation after the particle size is larger than 40 μm. An analysis of the graph's trend indicates that a D_i/D_c range of 0.3 to

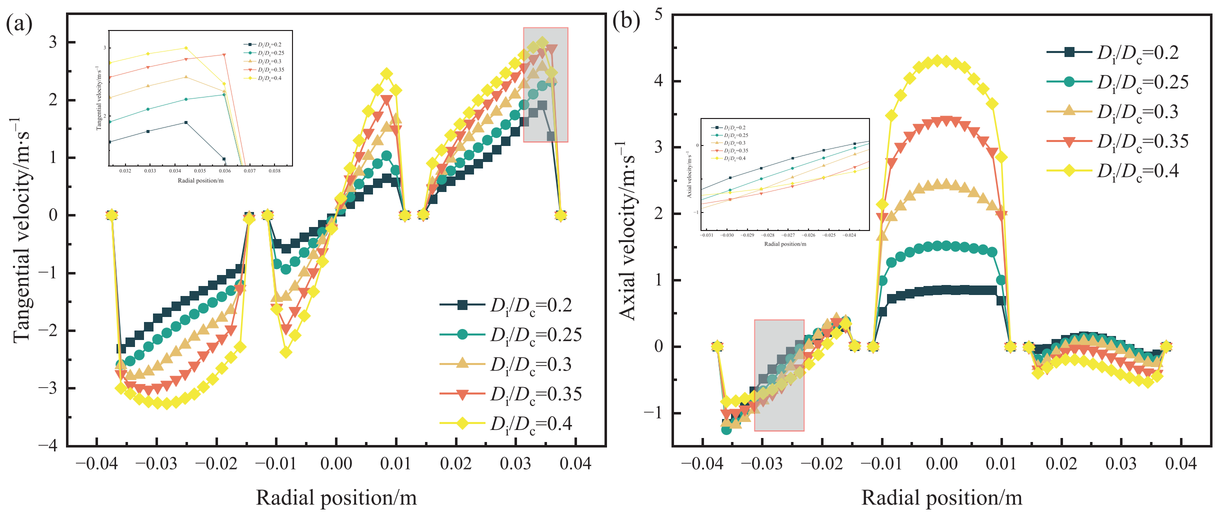

Fig. 10. Effects of inlet diameter on flow field distribution: (a) tangential velocity and (b) axial velocity.

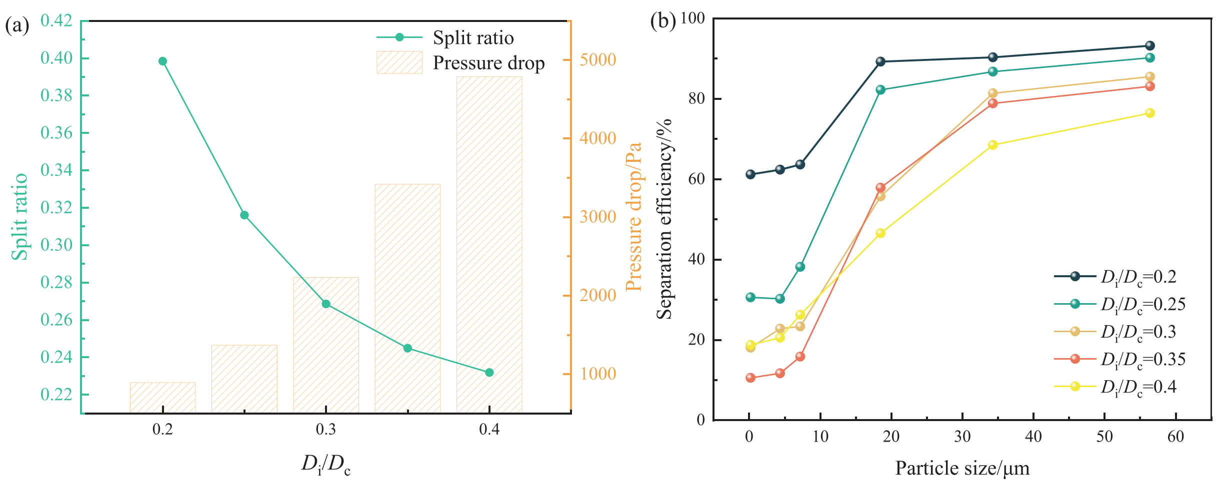

Fig. 11. Comparisons of (a) split ratio, pressure drop and (b) particle classification accuracy at different inlet diameters.

0.35 allows the cyclone separator to maintain a high separation efficiency while avoiding turbulence instability and equipment wear brought on by high pressure. This range is appropriate for a variety of particle sizes.

4.3.2. Effects of D_e

The tangential velocity diagrams indicate that smaller D_e/D_c ratios (*e.g.*, 0.3 and 0.35) enhance the separation efficiency of gas–liquid–solid multiphase flow. These ratios strengthen the combined effect of tangential and axial flow. Conversely, at higher D_e/D_c ratios (*e.g.*, 0.45 and 0.5), the peak tangential velocity decreases, weakening the centrifugal force field and reducing the effectiveness of radial particle separation. Additionally, larger ratios may weaken the axial downward velocity, particularly in the central region, potentially lowering the settling velocity of particles. Consequently, higher D_e/D_c ratios can hamper the formation of an efficient separation flow field in both axial and tangential directions, diminishing cyclone separator performance. The optimal D_e/D_c ratio, based on the analysis of velocity diagrams, lies between 0.3 and 0.35, promoting a strong downward flow to effectively facilitate particle separation (Fig. 12).

The cyclone separator's diverter ratio and pressure drop change with D_e/D_c values. As D_e/D_c increases, both the diverter ratio and pressure drop decrease. The split ratio, which is the amount of fluid entering the bottom opening compared to the total volume, indicates less heavy material is released when it is lower. A smaller pressure drop means less drag in the system (Fig. 13(a)).

Increasing D_e/D_c reduces internal fluid flow resistance, but this can also lower separation performance due to weaker centrifugal forces. Stronger centrifugal force, usually linked to larger pressure drops, improves the separation of mixtures.

For effective separation, balance the split ratio and pressure drop at a D_e/D_c ratio of 0.35. This ratio ensures a stable flow field and strong separation forces. Larger particles achieve about 98.51% separation efficiency, while smaller particles are harder to separate (Fig. 13(b)).

To enhance multiphase separation, keep the overflow pipe diameter small to meet flow requirements and improve small particle separation. A D_e/D_c ratio between 0.35 and 0.4 is ideal for balancing effective separation and energy use.

4.3.3. Effects of L_e

The effect of varying overflow tube insertion depths (L_e/D_c) on the cyclone separator's flow field is shown in Fig. 14. As L_e/D_c increases, the peak tangential velocity strengthens and converges towards the inner diameter, enhancing solid–liquid separation by

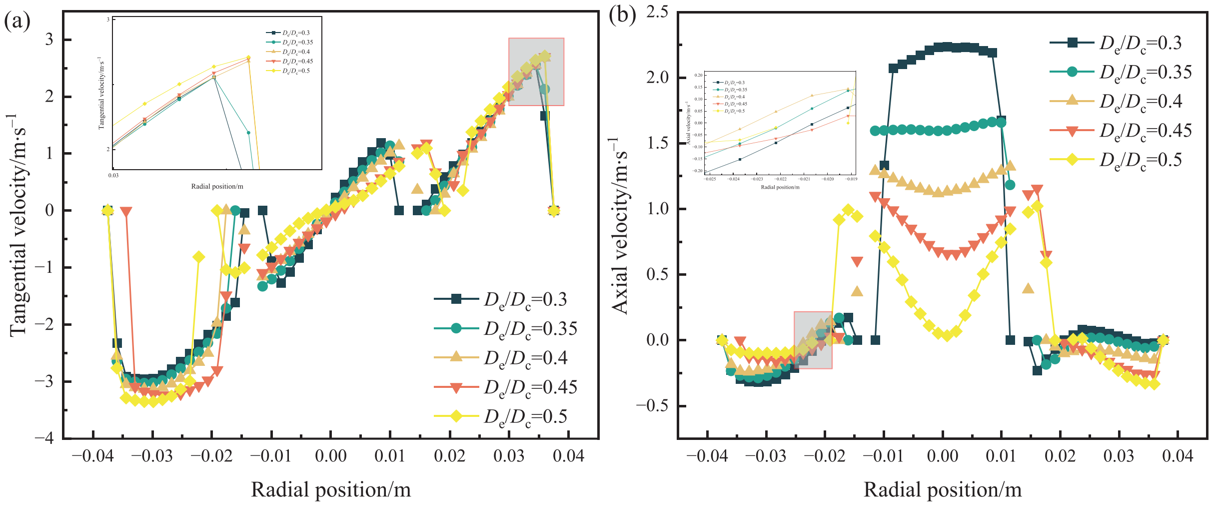

Fig. 12. Effects of overflow pipe diameter on flow field distribution: (a) tangential velocity and (b) axial velocity.

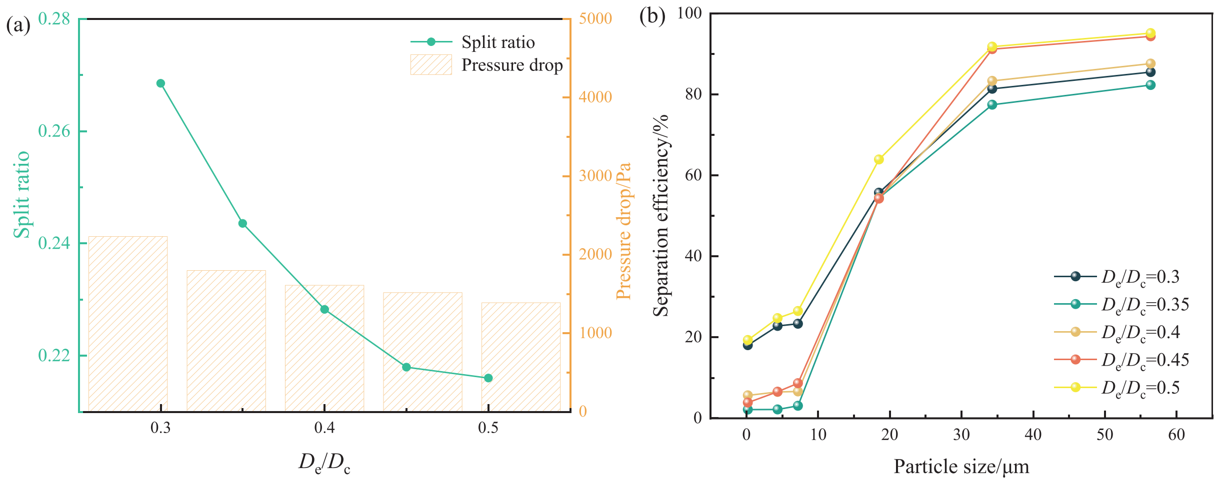

Fig. 13. Comparisons of (a) split ratio, pressure drop and (b) particle classification accuracy under different overflow pipe diameters.

increasing centrifugal force. However, excessively high tangential velocities may cause flow instability. The peak axial velocity also rises with L_e/D_c, accelerating the expulsion of lighter phases but potentially causing fluid entrainment and turbulence. A L_e/D_c ratio between 0.5 and 1.0 optimizes centrifugal force and separation efficiency while maintaining flow stability and reducing liquid entrainment.

Fig. 15(a) demonstrates that deeper overflow pipe insertion improves the split ratio, particularly at $L_e/D_c = 1.0$, enhancing diversion efficiency. However, higher insertion depths lead to slight pressure increases, which may affect fluid momentum and cyclonic strength, possibly raising energy consumption. As shown in Fig. 15(b), separation efficiency improves with particle size when L_e/D_c is small (*e.g.*, 0.2, 0.35), but efficiency for larger particles is suboptimal. With a moderate insertion depth, separation efficiency is optimized across a wider particle size range, particularly when L_e/D_c reaches 0.4–0.5. The ideal L_e/D_c ratio lies between 0.5 and 0.75.

4.3.4. Effects of D_z

Fig. 16 illustrates the effect of varying cone diameters on the cyclone separator's flow field. As the inner cone diameter increases, higher rotational velocities are generated, which strengthens the centrifugal force, helping larger particles move toward the outer wall and exit through the bottom flow opening. However, larger cone diameters also increase axial velocities, promoting upward fluid motion along the center. Small particles, which rely on axial velocity for upward discharge, are sensitive to these changes. If the axial velocity is too high, larger particles may be carried with the overflow fluid, reducing separation accuracy.

Fig. 17(a) shows how the inner cone diameter (D_z/D_c) affects the split ratio and pressure drop. The pressure drop remains relatively stable within a certain range of D_z/D_c, indicating that structural changes have minimal impact on energy loss. As D_z/D_c increases, the diverter ratio increases, particularly above $D_z/D_c = 0.6$, improving fluid discharge at the overflow port and satisfying particle classification needs. Fig. 17(b) demonstrates that larger cone diameters improve separation efficiency for larger particles, but the effect on large particles (>30 μm) diminishes. For smaller particles (10–20 μm), smaller cone diameters ($D_z/D_c = 0.2$ and 0.35) enhance separation efficiency. In terms of energy consumption, D_z/D_c between 0.65 and

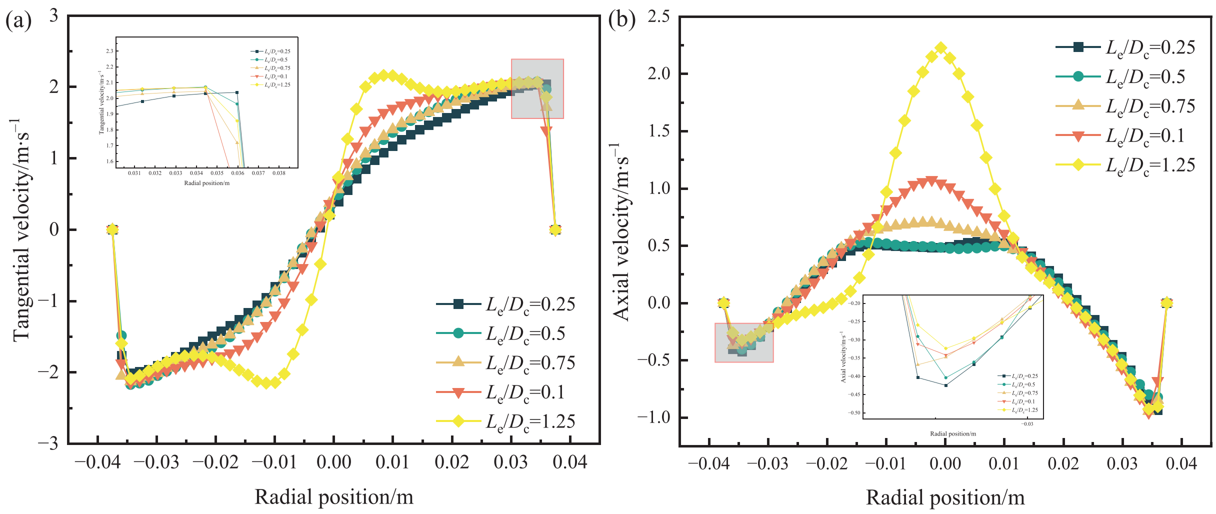

Fig. 14. Effects of overflow pipe insertion depth on flow field distribution: (a) tangential velocity and (b) axial velocity.

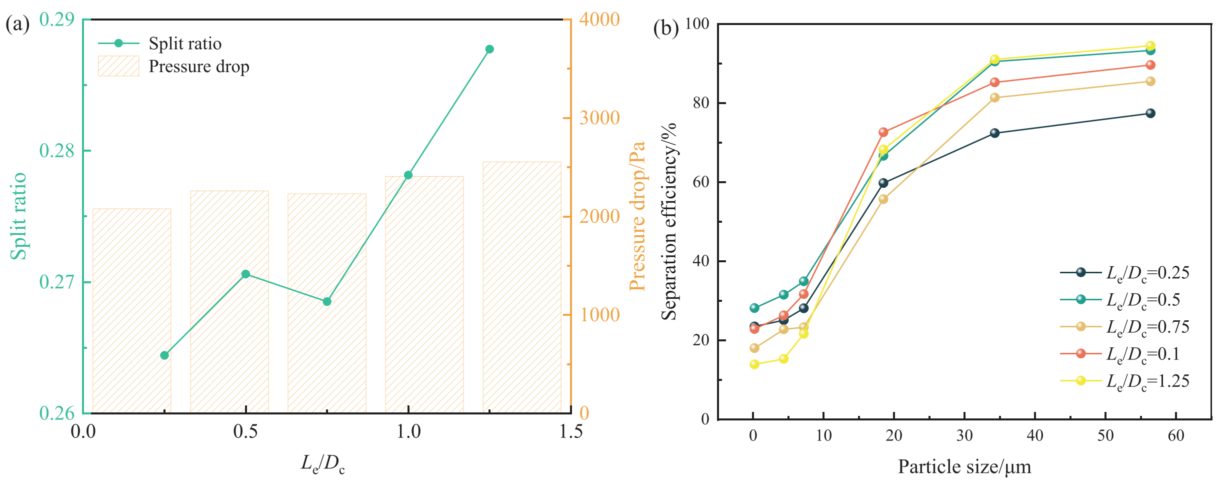

Fig. 15. Comparisons of (a) split ratio, pressure drop and (b) particle classification accuracy at different overflow pipe insertion depths.

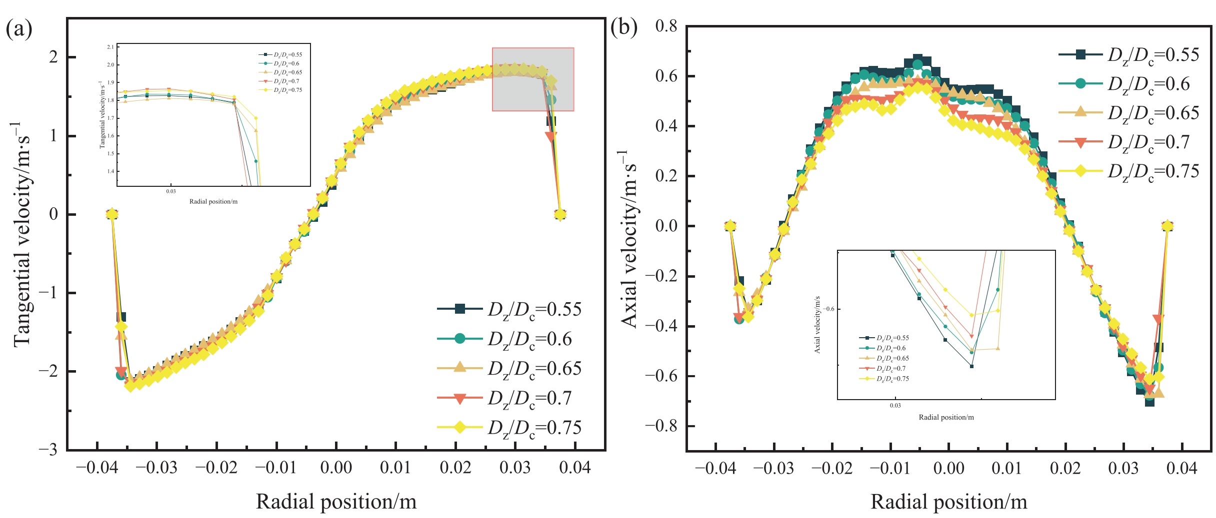

Fig. 16. Effects of cone diameter on flow field distribution: (a) tangential velocity and (b) axial velocity.

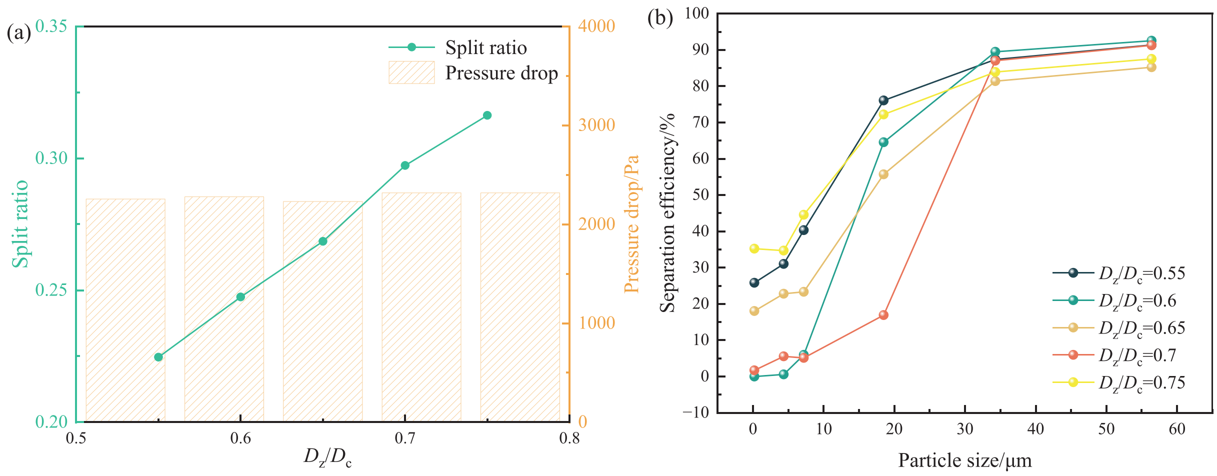

Fig. 17. Comparisons of (a) split ratio, pressure drop and (b) particle classification accuracy under different inner cone diameters.

0.75 optimizes overflow separation while meeting separation requirements.

5. Conclusions

This study presents a comprehensive numerical simulation of the internal flow field and separation performance of an inner cone cyclone desander. The investigation focuses on the effects of key structural parameters on the cyclone separator's performance, including D_i, D_e, L_e, and D_z. By analyzing particle motion behavior and mechanical forces, this research reveals the substantial impact of fluid dynamics and geometry-induced turbulence on the separator's performance, particularly on cut-size particles. The study provides the following key findings:

A smaller D_i enhances tangential velocity and centrifugal force, promoting fine particle separation. The optimal range for D_i/D_c is between 0.35 and 0.4.

A larger D_e favors the discharge of fine particles and reduces pressure drop, although it affects the separation of larger particles. The recommended D_e/D_c range is 0.25 to 0.35.

A deeper L_e increases the discharge of smaller particles but may cause turbulence, affecting separation efficiency. The optimal range for L_e/D_c is between 0.5 and 0.75, balancing overflow and bottom flow.

A smaller D_z increases centrifugal force, improving fine particle separation, though excessive reduction may cause instability. The recommended D_z/D_c range is between 0.6 and 0.65 to stabilize the flow field and ensure effective particle separation.

The single-factor analysis applied in this study offers a clear understanding of the independent effects of each parameter on separation performance. By isolating the influence of individual parameters, the approach simplifies experimental design and simulation, reducing computational complexity. However, the single-factor method is limited in its ability to address the complex interactions between multiple parameters. To overcome this limitation, multi-factor analysis (*e.g.*, response surface methodology) will be employed in future studies to explore the synergistic effects of various parameters, which is essential for optimizing the cyclone separator's overall performance.

The results of this research contribute to the design and optimization of cyclone separators, providing a foundation for future investigations that will include more complex multi-factor analysis to achieve enhanced performance in industrial applications.

CRediT Authorship Contribution Statement

Jie Kou: Writing – review & editing, Validation, Data curation. Hang Qiu: Writing – original draft, Software, Formal analysis. Chenyang Wang: Writing – original draft, Data curation, Conceptualization.

Availability of Data and Materials

The datasets used and analyzed during the current study are available from the corresponding author on reasonable request.

Declaration of Competing Interest

The authors have no relevant financial or non-financial interests to disclose.

Acknowledgement

This work is supported by the National Natural Science Foundation of China (52074341).

References

[1] Y.C. Liu, Q.X. Cheng, B. Zhang, F. Tian, Three-phase hydrocyclone separator—A review, *Chem. Eng. Res. Des.* 100 (2015) 554–560.
[2] H. Yoshida, K. Ono, K. Fukui, The effect of a new method of fluid flow control on submicron particle classification in gas-cyclones, *Powder Technol.* 149 (2–3) (2005) 139–147.
[3] H. Chen, J. Zhang, S. Liu, J.Y. Xu, Liquid–solid two-phase flow and separation behavior in a novel cyclone separator, *Phys. Fluids* 36 (6) (2024) 063304.
[4] J.X. Yang, G.G. Sun, C.Z. Gao, Effect of the inlet dimensions on the maximum-efficiency cyclone height, *Sep. Purif. Technol.* 105 (2013) 15–23.
[5] K. Elsayed, C. Lacor, The effect of cyclone inlet dimensions on the flow pattern and performance, *Appl. Math. Model.* 35 (4) (2011) 1952–1968.
[6] Z.W. Zhang, Q. Li, Y.H. Zhang, H.L. Wang, Simulation and experimental study of effect of vortex finder structural parameters on cyclone separator performance, *Sep. Purif. Technol.* 286 (2022) 120394.
[7] X.L. Yang, J.T. Yang, S.B. Wang, Y.M. Zhao, Effects of operational and geometrical parameters on velocity distribution and micron mineral powders classification in cyclone separators, *Powder Technol.* 407 (2022) 117609.
[8] M.H. Jiang, W. Jiang, G.Y. Zhang, Y. Zhang, X.J. Wang, Structural design and testing of hydrocyclones for fine particle separation, *J. Daqing Pet. Inst.* 1 (2005) 58–60. (in Chinese)
[9] Y. Fang, Influence of hydrocyclone structural parameters on its performance, *Guangdong Chem. Ind.* 32 (10) (2005) 26–30. (in Chinese)
[10] K. Elsayed, C. Lacor, Optimization of the cyclone separator geometry for minimum pressure drop using mathematical models and CFD simulations, *Chem. Eng. Sci.* 65 (22) (2010) 6048–6058.

[11] L.S. Brar, R.P. Sharma, K. Elsayed, The effect of the cyclone length on the performance of stairmand high-efficiency cyclone, *Powder Technol.* 286 (2015) 668–677.

[12] R. Shastri, L.S. Brar, Numerical investigations of the flow-field inside cyclone separators with different cylinder-to-cone ratios using large-eddy simulation, *Sep. Purif. Technol.* 249 (2020) 117149.

[13] R. Shastri, R.P. Sharma, L.S. Brar, Numerical investigations of cyclone separators with different cylinder-to-cone ratios, *Part. Sci. Technol.* 40 (3) (2022) 337–345.

[14] R.B. Xiang, K.W. Lee, Numerical study of flow field in cyclones of different height, *Chem. Eng. Process. Process. Intensif.* 44 (8) (2005) 877–883.

[15] J. Gimbun, T.G. Chuah, T.S.Y. Choong, A. Fakhru'l-Razi, Prediction of the effects of cone tip diameter on the cyclone performance, *J. Aerosol Sci.* 36 (8) (2005) 1056–1065.

[16] O. Hamdy, M.A. Bassily, H.M. El-Batsh, T.A. Mekhail, Numerical study of the effect of changing the cyclone cone length on the gas flow field, *Appl. Math. Model.* 46 (2017) 81–97.

[17] I.C. Bicalho, J.L. Mognon, J. Shimoyama, C.H. Ataíde, C.R. Duarte, Effects of operating variables on the yeast separation process in a hydrocyclone, *Separ. Sci. Technol.* 48 (6) (2013) 915–922.

[18] S.B. Kuang, K.W. Chu, A.B. Yu, A. Vince, Numerical study of liquid–gas–solid flow in classifying hydrocyclones: effect of feed solids concentration, *Miner. Eng.* 31 (2012) 17–31.

[19] L.M. Tavares, L.L.G. Souza, J.R.B. Lima, M.V. Possa, Modeling classification in small-diameter hydrocyclones under variable rheological conditions, *Miner. Eng.* 15 (8) (2002) 613–622.

[20] T. Neesse, J. Dueck, H. Schwemmer, M. Farghaly, Using a high pressure hydrocyclone for solids classification in the submicron range, *Miner. Eng.* 71 (2015) 85–88.

[21] H.X. Yuan, J.F. Yu, H.B. Liu, Effect of diverter ratio on the basic performance of oil-water separation cyclones, *Petro. Machin.* 9 (2000) 17–20. (in Chinese)

[22] S. Chandrakant R., A. Kulkarni, R.V. Sawant, A.K. Pandey, H. Panchal, K.K. Sadasivuni, A. Kumar, Numerical simulation of cascaded cyclone separator for nanosize aerosol, *Energy Sources Part A Recov. Utiliz. Environ. Eff.* 41 (1) (2021) 11042–11062.

[23] J.C. Cullivan, R.A. Williams, R. Cross, Understanding the hydrocyclone separator through computational fluid dynamics, *Chem. Eng. Res. Des.* 81 (4) (2003) 455–466.

[24] W.K. Evans, A. Suksangpanomrung, A.F. Nowakowski, The simulation of the flow within a hydrocyclone operating with an air core and with an inserted metal rod, *Chem. Eng. J.* 143 (1–3) (2008) 51–61.

[25] M. Narasimha, M.S. Brennan, P.N. Holtham, T.J. Napier-Munn, A comprehensive CFD model of dense medium cyclone performance, *Miner. Eng.* 20 (4) (2007) 414–426.

[26] Z. Zheng, L.X. Zhao, M.H. Jiang, M. Zhang, Simulation analysis and experimental study on hydrocyclone with new structure of overflow pipe, *Petrochem. Equip.* 40 (5) (2011) 5–8. (in Chinese)

[27] Z.C. Wang, W.Q. Chen, M.H. Jiang, X.M. Liu, L.X. Zhao, Optimal design of dynamic hydrocyclone structure parameters, *J. Petrol.* 22 (4) (2001) 104–107. (in Chinese)

[28] S.Y. Jiang, S.F. Yang, A cyclone with conveniently adjustable size of underflow port, Chinese pat., CN 201120021608.4, 2011-07-17. (in Chinese)

[29] P. Zhang, X.F. Zhang, M.Q. Fan, Experimental study and numerical simulation of cyclone underflow orifice regulation method, *Mining Machin.* 42 (4) (2014) 78–82. (in Chinese)

[30] Y. Xue, F.S. Yan, X.Z. Hu, J.X. Shi, K. Zheng, Numerical study of three-dimensional gas-phase flow field of cyclone separator based on RSM model, *Metall. Energ.* 40 (1) (2021) 29–34, 38. (in Chinese)

[31] R.A. Johnson, W.E. Gibson, D.R. Libby, Performance of liquid–liquid cyclones, *Ind. Eng. Chem. Fund.* 15 (2) (1976) 110–115.

[32] L.H. Wu, Performance study of folded angle inlet, round platform outlet and straight cylinder cyclone separator, Ph.D. Thesis, Zhejiang University, China, 2016. (in Chinese)

[33] S.Q. Tang, Research on the influence of performance parameters of cyclone separator based on CFD, Ph.D. Thesis, Shandong University of Technology, China, 2015. (in Chinese)

[34] M.H. Jiang, F. Tan, S.Q. Jin, G.L. Long, G.Q. Chen, B.R. Xu, Shape optimisation of cyclone based on fluent mesh deformation, *Adv. Chem. Eng.* 35 (8) (2016) 2355–2361. (in Chinese)

[35] B. Tang, Research and structural design of cyclone separation process based on particle motion behavior regulation, Ph.D. Thesis, East China University of Science and Technology, China, 2016. (in Chinese)